Advanced Energy and Sustainability Research

ADVANCED ENERGY & SUSTAINABILITY RESEARCH Open Access

www.advenergysustres.com

RESEARCH ARTICLE OPEN ACCESS

Effects of Manufacturing-Induced Initial Material State and Lamination Duration on Thermomechanical Properties of Photovoltaic Encapsulants

Nikolina Pervan[1,2,3] | Jutta Geier[1,2] | Michael Daenen[3,4,5] | Gernot Oreski[1,2]

[1]Polymer Competence Center Leoben GmbH (PCCL), Leoben, Austria | [2]Materials Science and Testing of Polymers, Technical University of Leoben, Leoben, Austria | [3]UHasselt Institute for Materials Research (IUMAT), Hasselt, Belgium | [4]imec, IUMAT, Genk, Belgium | [5]EnergyVille, IUMAT, Genk, Belgium

Correspondence: Nikolina Pervan (nikolina.pervan@pccl.at) | Gernot Oreski (gernot.oreski@pccl.at)

Received: 6 May 2026 | **Revised:** 6 August 2026 | **Accepted:** 10 August 2026

Keywords: crosslinking degree | CTE | EPE | PV encapsulants | thermomechanical behaviour

ABSTRACT

Encapsulants are vital for the structural integrity and protection of photovoltaic (PV) modules, yet the impact of processing history and crosslinking on their thermomechanical behaviour is often oversimplified in numerical simulations. This study experimentally investigates how lamination conditions affect six encapsulant types, including crosslinking (EVA, POE), noncrosslinking (TPO), and coextruded (EPE) materials. The crosslinking behaviour was characterized using differential scanning calorimetry (DSC) and Fourier transform infrared spectroscopy (FTIR), while thermomechanical properties were assessed via digital image correlation. Results indicate that conventional DSC-based methods for the calculations of degree of crosslinking, while standard for EVA, have significant limitations when applied to multilayer encapsulants. Fourier transform infrared spectroscopy in attenuated total reflection mode combined with principal component analysis proved to be an effective, rapid method for qualitative clustering of crosslinked encapsulants. The findings reveal that manufacturing history strongly influences prelamination behaviour, even for the materials labelled under the same commercial nomenclature. Increased lamination duration drives encapsulants toward more isotropic coefficients of thermal expansion (CTE), with noncrosslinking materials reaching final CTE values faster. The presented dataset may support future investigations of stress development, thermomechanical interactions, and material selection in conventional and emerging PV module architectures.

1 | Introduction

With the continuous rise in photovoltaic (PV) module installations, the decrease of module prices, and the rapid evolution of solar cell technologies, material selection within the PV module stack continues to be a critical factor for its long-term reliability [1–6]. According to ITRPV, performance warranties are extending toward 30 years, while module architectures and bill of materials are undergoing significant transitions [1] without the knowledge on long-term performance of the new module designs. In particular, the industry is moving from glass/backsheet to glass/glass module designs, from p-type to n-type, perovskite, and silicon-perovskite tandem solar cells, and from the long-established ethylene vinyl acetate (EVA) encapsulant toward alternative materials such as polyolefin (POE), thermoplastic polyolefin (TPO), and coextruded EVA-POE-EVA (EPE) encapsulants [1, 2, 7, 8].

The rapid expansion of PV modules has also come upon land availability limitations, particularly in densely populated or mountainous regions where large field-deployed installations are constrained [9–11]. This has driven the development of

alternative deployment strategies that generate electricity without competing with conventional land use. Examples include agrivoltaics [12], floating PV systems [13], and various integrated photovoltaics (IPV), such as building-integrated photovoltaics [14] and vehicle-integrated photovoltaics [15], where many PV module designs rely on advanced polymer-based materials that enable lightweight structures, flexible geometries, and adaptable module architecture.

These developments place new demands on the performance and stability of polymeric materials used in PV modules. For instance, n-type and perovskite solar cells exhibit sensitivity to moisture, while in glass-free PV designs, the moisture barrier often needs to be further supported by the encapsulant layer [16–20]. In addition, perovskite and tandem devices can be prone to delamination during or after lamination due to mismatches in thermomechanical properties [21, 22].

Encapsulants play a central role in the mechanical and structural integrity of PV modules. Beyond providing optical coupling and electrical insulation, they embed and connect solar cells with the rest of the stack, reduce moisture ingress, and minimize transfer of the stresses between module components induced by environmental loading [23, 24]. Among all components in a glass/glass PV module, the encapsulant is the only soft, polymeric layer and therefore governs how the module responds to thermal and mechanical loads. Daily and seasonal thermal cycling leads to repeated expansion and contraction of the PV stack components, resulting in stresses caused by coefficient of thermal expansion (CTE) mismatches between glass, solar cells, interconnects, and polymer layers [25, 26]. While the glass layer in conventional modules helps constrain dimensional changes of the encapsulants in the stack, the situation is different for flexible, lightweight, or glass-free IPV module designs. In these cases, even relatively small expansion or contraction of the polymer layers may lead to larger warping or deformation of the module. If not properly managed, these stresses can contribute to failure modes such as solar cell cracking, solder joint fatigue, delamination, and in the case of mechanically sensitive technologies such as perovskites, solar cell layer delamination and device failure [21, 22, 26–29].

Thermomechanical behaviour of polymers has been extensively studied in other technological fields, including automotive, microelectronics, packaging, and medical applications [30–39]. In contrast, experimental investigations focusing on the thermomechanical properties of PV polymeric components, including encapsulants, remain limited [40–45]. Many studies addressing thermomechanical effects in PV modules rely primarily on numerical simulations, in which encapsulant behaviour is often simplified to facilitate modeling or sometimes even ignored [46]. Common assumptions include linear elastic material behaviour and often assumed constant CTE at 270 ppm over broad temperature ranges, frequently based on EVA as a reference material [47–53]. While researchers introduced viscoelastic material descriptions to better capture encapsulants behaviour [43, 49, 54], constant CTE values are still widely used. As a result, experimentally observed material behaviour may not be fully represented in thermomechanical simulations.

In reality, the thermomechanical response of polymer materials is strongly influenced by their processing history [33]. However, systematic experimental studies addressing the impact of encapsulant processing history on thermomechanical properties are scarce [55]. Polymer morphology, crystallinity, and dimensional stability are affected by manufacturing conditions (extrusion temperature and speed, stretching in both machine direction (MD) and transverse direction (TD), speed of cooling down, and annealing process) prior to lamination [31, 33, 40, 56]. These factors are known to influence the initial material state and may contribute to differences in dimensional stability observed after lamination (as shown in Figure 1).

On the other hand, lamination temperature, pressure, dwell time, and cooling conditions determine the extent to which initial processing history is overwritten and new polymer networks and chain orientations are formed [41]. These parameters are of great importance for minimizing residual stresses, which can impact PV module reliability during operation [51, 58]. For crosslinking encapsulants, the degree of crosslinking represents an additional impacting parameter on encapsulants properties in the PV module. Previous studies have demonstrated methods for determining the degree of crosslinking [59–70] and the importance of its impact on adhesion, discoloration, corrosion, and potential-induced degradation in PV modules [58, 71–75]. In contrast, the influence of the degree of crosslinking on thermomechanical properties, particularly on CTE behaviour, has received little attention [76]. On top of that, for noncrosslinking encapsulants such as TPO, the absence of a defined curing reaction raises fundamental questions regarding

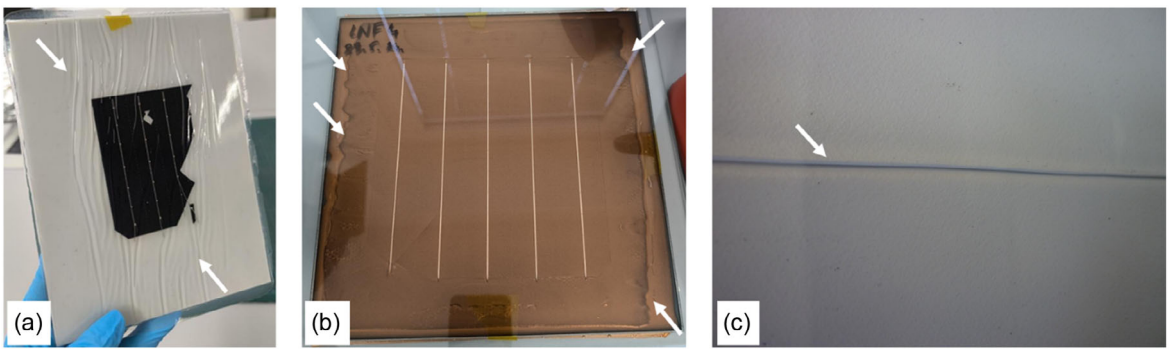

FIGURE 1 | Examples of defects created during the lamination of PV modules caused by high encapsulant shrinkage: (a) wrinkles in the frontsheet (in-house lamination), (b) back encapsulant shrinking (in-house lamination), and (c) wrinkle in the backsheet [57].

how sufficient lamination conditions should be defined to ensure long-term reliability.

This work addresses mentioned gaps by experimentally investigating the effect of processing history and lamination duration on the thermomechanical properties of PV encapsulants. A total of six encapsulant materials, including crosslinking EVA, two crosslinking POE types, a noncrosslinking TPO, and two coextruded EPE, were studied under multiple lamination conditions. The degree of crosslinking was characterized using destructive (differential scanning calorimetry (DSC)) and nondestructive (Fourier transform infrared spectroscopy (FTIR)) techniques, and thermomechanical behaviour was assessed using digital image correlation (DIC). By comparing the initial and postlamination thermomechanical behaviour of commercially relevant encapsulants under controlled lamination conditions, this study provides experimental insight into the influence of the initial material state and lamination duration on encapsulant behaviour relevant to current and emerging PV module technologies.

2 | Materials and Methods

The experimental investigation was carried out on six commercially available PV encapsulant materials produced by different manufacturers. The encapsulants are referred to anonymously throughout the text to avoid bias or brand-specific interpretation. The study included an industry-standard EVA, followed by two crosslinking POEs, one noncrosslinking TPO, and two EPE encapsulants. The two EPE encapsulants differed with their POE core type, EPE-1 had a noncrosslinking and the EPE-2 crosslinking POE core. An overview of the investigated materials is provided in Table 1. For each encapsulant type, a roll of ≈10 m in length was available. From each roll, two specimens with dimensions of 20 x 20 cm^2 were cut from random positions along the roll length in order to account for potential in-roll material variability. The degree of crosslinking and thermomechanical properties of all encapsulants were investigated in both unlaminated (uncured) and laminated (cured) states. The lamination process and parameters are described in the Supporting Information.

2.1 | DSC

DSC was performed using a DSC 4000 from PerkinElmer Inc. to measure thermograms of encapsulants. Approximately 7 mg of each material was placed in an aluminium pan with perforated lid. For each material, three measurements were performed, and the average of these measurements was used for the calculations. DSC measurements were carried out in accordance with IEC 62788-1-6:2017 for the combined enthalpy and melt/freeze method [77]. According to this standard, the degree of crosslinking of EVA-based encapsulants can be determined from the residual curing enthalpy and from changes in the crystallization behaviour. In the work of [70], the method was proven to be suitable for determination of crosslinking degrees of POE encapsulants. In the present study, the same methodology was applied to all crosslinking encapsulants investigated, and details of the DSC measurement parameters are described in Supporting Information.

2.2 | FTIR and Principal Component Analysis (PCA)

Fourier transform infrared spectroscopy in attenuated total reflection mode (FTIR-ATR) was applied as a nondestructive method to investigate the crosslinking behaviour of the encapsulant materials. This method was chosen as it enables possible observation of small chemical differences between materials that might have been below limit of detections of the destructive methods studied here. FTIR-ATR measurements were performed using a SpectrumTwo spectrometer (PerkinElmer, Inc., USA) equipped with a Quest ATR unit with diamond crystal (Specac Ltd., United Kingdom). Three spectra per sample were recorded over a wavenumber range of 4000–650 cm^{-1} at a resolution of 4 cm^{-1}, with each spectrum representing the average of four scans.

The obtained FTIR-ATR spectra were analysed by PCA. PCA is an exploratory multivariate statistical method that reduces the dimensionality of complex datasets while preserving most of the original variation [78, 79]. In this study, PCA was used as a visualisation tool to reveal spectral trends, sample groupings, and changes related to the degree of crosslinking. In general, PCA reduces the dimensionality of the dataset by generating a smaller number of new variables, referred to as principal components (PCs), which retain most of the variation present in the original data. The first principal components account for the largest share of the total variance. In this study, score plots of the first two components (PC1 and PC2) were used to assess possible trends within the sample sets. PC1 represents the direction of the greatest spectral variation, while PC2 represents the second-largest variation. The position of each point in the score

TABLE 1 | Studied encapsulant materials and their properties.

Encapsulant	Polymer type	Crosslinking chemistry	Thickness, µm
EVA	Ethylene vinyl acetate[a]	Peroxides	600
POE-1	Ethylene α-olefin[a]	Peroxides	450
POE-2	Ethylene α-olefin[a]	Peroxides	500
TPO	Ethylene ethyl acrylate[a]	Noncrosslinking	400
EPE-1	EVA—ethylene acrylate copolymer—EVA [8]	Peroxides for EVA layers	450
EPE-2	EVA—ethylene α-olefin—EVA [8]	Peroxides	600

[a]In house measured and identified using FTIR-ATR.

plot therefore reflects its spectral similarity to or difference from the other points. Points located close together have similar spectral information, whereas greater distances indicate larger spectral differences. Prior to PCA, the spectra were preprocessed by standard normal variate normalization and first-derivative transformation using a Savitzky Golay filter with smoothing. In addition, mean centering was applied before PCA. The PCA results were then compared with the findings of the other methods used in this study.

2.3 | DIC—CTE

The dimensional stability of the unlaminated samples and CTE of the unlaminated and laminated samples were measured using a Dantec Q400 TCT DIC system from Dantec Dynamics. The device consists of two cameras and a temperature-controlled chamber equipped with a heated/cooled thermal plate. During measurement, a time series of images of the sample surface is taken during the thermal stages. The recorded images were evaluated using Istra 4D software (Dantec Dynamics), which calculates the relative surface displacement by correlating each image in the series with the initial reference image. The measurements were done in the temperature range from 20 to 120 °C with a heating rate of 2 °C min^{-1}. For the dimensional stability of the unlaminated encapsulants, the length change in both the MD and TD was followed relative to the initial diameter of 20 mm, taken from the centre of each sample. Details of sample dimension and preparation are provided in the SI.

3 | Results and Discussion

3.1 | The Crosslinking Behaviour and Degree of Crosslinking From DSC

As mentioned, according to IEC 62788-1-6:2017, the degree of crosslinking of EVA-based encapsulants can be determined from the residual curing enthalpy and from changes in crystallization behaviour [70, 80, 81]. In this study, the same heating profile was applied to all encapsulants, and the degree of crosslinking was calculated following the equations provided in the standard [77].

The first cooling and second heating curves are particularly important as they provide the information required for the calculation of the degree of crosslinking. Therefore, these curves were carefully analysed and compared. Calculated values for the degree of crosslinking from enthalpy (G_e) and melt/freeze (G_{MF}) methods are presented in Table 2. Due to the large amount of data, Figures 2 and 3 show only the DSC curves for POE-1, EPE-1, and EPE-2; the remaining curves for the other encapsulants are provided in the Supporting Information together with graphs showing the full heating range for all encapsulants at the lamination time of 15 min (Figures S4–S6).

For the EVA encapsulant, G_e values indicated lower degree of crosslinking compared to G_{MF} values. According to the change in the crystallization peak from the first cooling curves, a degree of curing of 96.4% (G_{MF}) was reached after 10 min of lamination, while G_e calculations showed a degree of crosslinking of only 63.6%. This may be attributed to incomplete peroxide decomposition or delayed degassing due to the excess peroxide content commonly added to ensure complete crosslinking, resulting in differences in the calculated degree of crosslinking [70, 80]. The observation is confirmed by the second heating curve, where an exothermic peak between 160 and 180 °C is still present at lamination duration of ≥10 min. While this may lead to misinterpretation of the crosslinking degree, it poses additional concern. Residual peroxides in combination with other additives can cause encapsulant yellowing and corrosion of PV module components [29, 82]. The apparent increase of G_{MF} above 100% for ≥15 min is likely an artefact resulting from small variations in crystallization behaviour, which are sensitive to the maximum heating temperature used in the DSC cycle. G_e is in steady increase and reaches a maximum value of 84% for 30 min lamination duration.

POE-1 exhibits the slowest curing behaviour among the studied single-layer encapsulants. Furthermore, a second melting peak at ≈104 °C is observed, likely from the presence of a small amount of the crystalline fraction from low-density polyethylene. An exothermic peak in the second heating curve remains visible up to a lamination time of 30 min, and a similar trend is observed in the crystallization peak during the first cooling. However, the calculated values of G_e and G_{MF} differ, the degree of crosslinking from the residual enthalpy is lower than the melt/freeze, 76.9% and 94.9%, respectively.

TABLE 2 | Crosslinking degrees calculated according to residual enthalpy (G_e) and melt/freeze method (G_{MF}).

Lamination time, min	EVA		POE-1		POE-2		EPE-1		EPE-2	
	G_e, %	G_{MF}, %	G_e, %	G_{MF}, %	G_e, %	G_{MF}, %	G_e, %	G_{MF}, %	G_e, %	G_{MF}, %
2	14.9	7.2	39.5	2.9	0	0[a]	0	0[a]	0	Dual peak
5	66.1	79.0	20.9	12.3	2.3	0[a]	10.5	1.3	34.6	
10	63.6	96.4	63.7	52.5	52.4	46.0	59.2	90.4	94	
12	66.1	99.3	58.2	50.2	64.3	66.1	67.1	110.7[b]	94.7	
15	77.7	101.7[b]	54.9	69.5	85.7	64.6	96.1	106.0[b]	96.2	
20	80.7	100.9[b]	67	88.1	85.7	63.8	93.4	103.3[b]	99	
30	84	101.7[b]	76.9	94.9	85.7	76.7	94.7	101.1[b]	97.7	

[a]False negative value.
[b]False positive value.

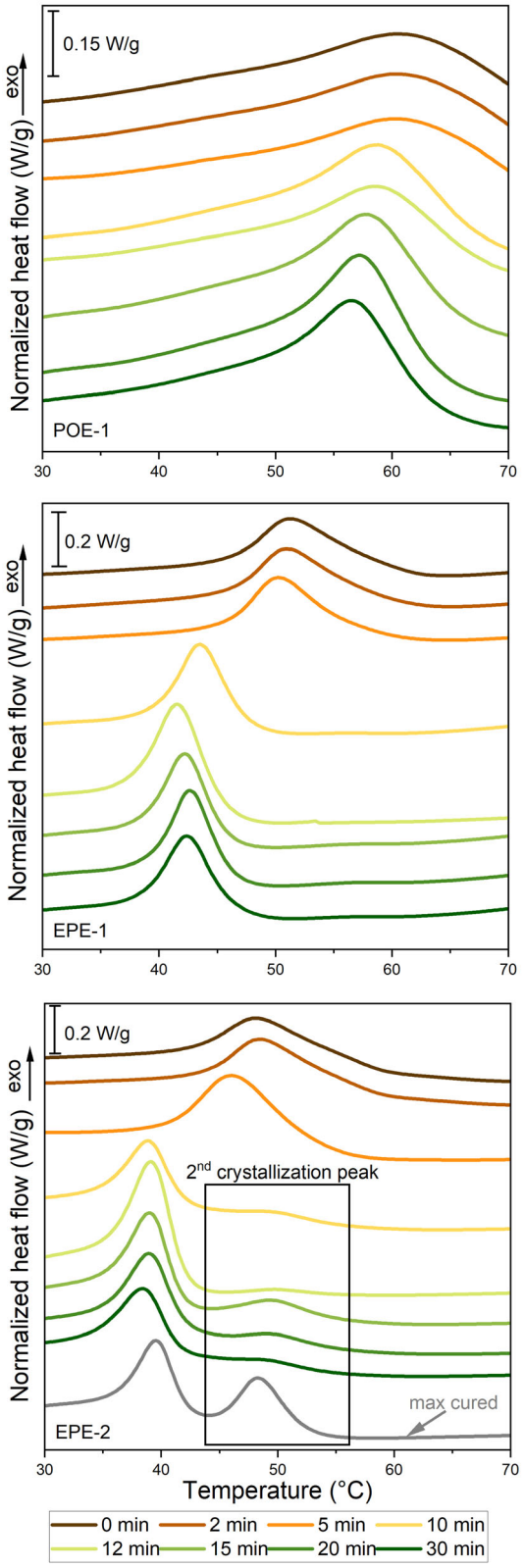

FIGURE 2 | The first cooling DSC curves of uncured and laminated POE-1, EPE-1, and EPE-2 in temperature range of 30–70 °C, where the crystallization peak is observed.

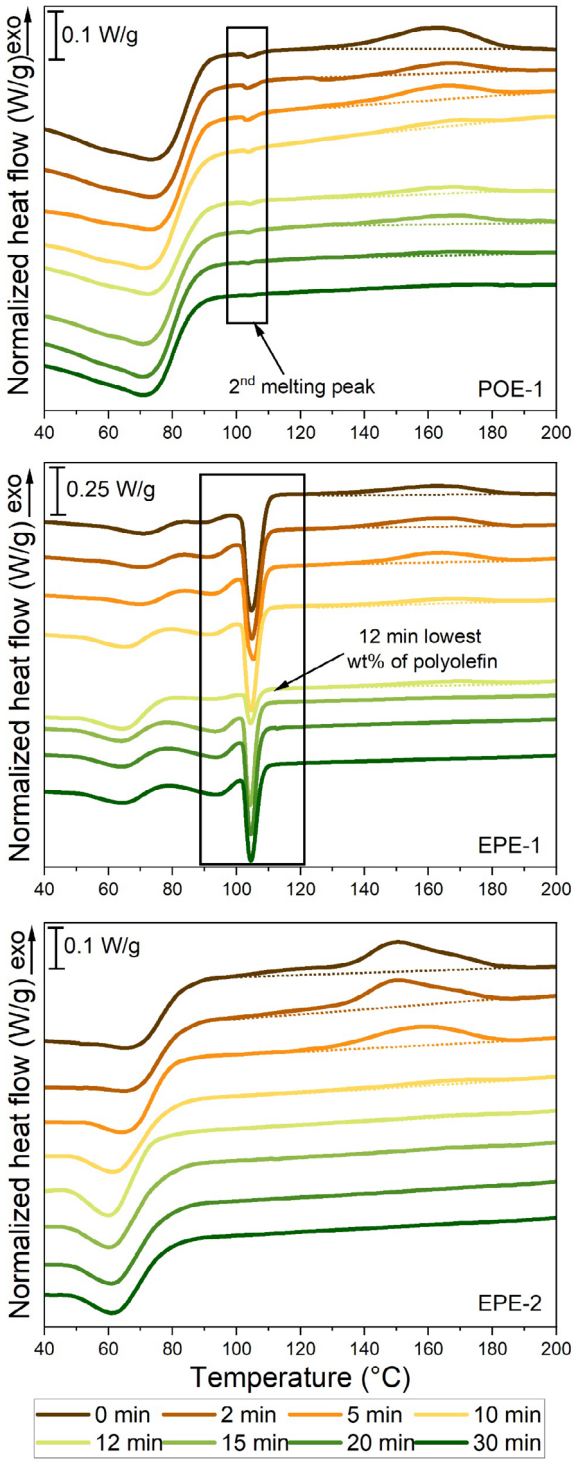

FIGURE 3 | The second heating DSC curves of uncured and laminated POE-1, EPE-1, and EPE-2. The dotted line indicates the thermogram baseline and aids in identifying the exothermic crosslinking peak.

POE-2 exhibits a relatively slow change in the crosslinking behaviour for lamination times below 10 min. Additionally, the false negative G_{MF} values are observed for 2 and 5 min lamination times. These values are likely related to differences in thermal history between extrusion and lamination of encapsulant, which can influence crystallization behaviour of the semi crystalline polymers when the degree of crosslinking is still low. However, additional investigations would be required to directly confirm this mechanism. A lamination duration of 15 min at 150 °C appears sufficient to ensure complete peroxide decomposition and to reach the maximum degree of curing for this material formulation. For lamination times ≥15 min, the

characteristic exothermic peak associated with peroxide-initiated crosslinking is no longer visible. However, a change in the baseline slope of the heat–flow curve within the same temperature interval indicates the presence of residual crosslinking reaction. Based on the residual enthalpy, the calculated degree of crosslinking stabilizes at ≈85% across all samples. Furthermore, the first cooling thermograms reveal a change in the crystallization peak for all specimens laminated for ≥15 min. This behaviour suggests that residual crosslinking reaction, observed in the second heating, continues beyond the primary peroxide-initiated stage.

Even though POE-1 and POE-2 differed in the speed of their crosslinking, for both of them, peroxides were decomposed before the maximum degree of curing could be reached (according to the G_{MF}) calculations. However, since POE encapsulants are generally considered a slow-curing material with a lower overall degree of crosslinking compared to EVA, the available peroxide content was most likely sufficient to reach the optimal degree of curing despite apparent differences in measurement [67].

As expected, TPO is a noncrosslinking encapsulant, and therefore, its thermal properties are independent of lamination duration.

A more complex crosslinking behaviour is observed for the EPE encapsulants. As mentioned previously, EPE-1 and EPE-2 differ in the nature of their POE core materials. In EPE-1, the POE core is a noncrosslinking type; therefore, the peroxides present in the material are intended solely for EVA crosslinking. Consequently, no changes in the melting or crystallization peaks of the POE core are observed. Analysis of the second heating curve revealed an unexpected deviation for the samples laminated for 12 min. All three tested specimens exhibited a lower apparent POE fraction compared to samples laminated for other durations. These specimens were taken from random positions within a single $20 \times 20\ cm^2$ laminated sample. Additional DSC measurements were performed on several specimens from the same laminate, and a reduced apparent POE content was consistently observed. This suggests that the effect is not related to measurement variability but rather to structural inhomogeneity within the laminate. A possible explanation is an uneven distribution of the POE layer within the laminated stack. To verify this assumption, cross-sections of the laminate were examined by optical microscopy. The images confirmed local variations in the POE layer distribution. Representative images are provided in the Supporting Information (Figure S3). For the crosslinking behaviour from the second heating curve, contrary to the single EVA encapsulant, the exothermic peak after 15 min of lamination duration is no longer observable. A similar trend is observed from the first cooling curves, where the crystallization peak for samples laminated for ≥15 min is influenced by the amount of POE core present, but no further crosslinking is observed.

EPE-2 exhibits distinctly different behaviour compared to EPE-1. In this material formulation, both the EVA and POE components are crosslinking polymers. For uncured and under-cured samples (0, 2, and 5 min lamination time), two exothermic peaks are observed, which could be attributed to the presence of different crosslinking systems [83]. In contrast to the measured single-layer EVA and POE samples, no exothermic peak is observed after 12 min of lamination, indicating that the peroxides have fully decomposed, and EPE-2 has reached an apparent degree of crosslinking of 94.7%. However, analysis of the first cooling curves, together with the cooling curve from the second cooling step, referring to the "maximum cured sample" (grey curve in Figure 2), shows that the crosslinking reaction is still ongoing, similar to the behaviour observed for POE-2. At this stage, heat acts as the main driving factor for further network formation, and the reaction proceeds slowly at 150 °C. This behaviour indicates that although the peroxides have decomposed, the curing process has not reached its maximum extent. Higher lamination temperatures or longer lamination times are therefore required to achieve a higher degree of curing in the POE core, as visible from the second cooling curve, where the crystallization peak associated with the POE phase appears with a higher intensity. The results suggest that the curing process did not reach its maximum extent under the investigated conditions.

In addition, even though the crosslinking reaction in EPE-2 proceeds slowly after peroxide decomposition, similar to POE-2, no baseline slope change is observed in the second heating curve. This low detectability of residual crosslinking reaction is due to the slow reaction rate, combined with the POE fraction representing only about one third of the total mass in a small sample size (≈7 mg). Additionally, the degree of curing could not be determined using the melt/freeze method, which is designed for encapsulants exhibiting a single crystallization peak. However, the presence of two crystallization peaks in EPE-2 prevents reliable calculation using this approach.

3.2 | Limitations of DSC Methods for Determining Degree of Crosslinking of EPE Encapsulants

Even though combined enthalpy and melt/freeze DSC methods have been used to evaluate degree of curing for EVA and POE encapsulants [70, 80, 81], applying these methods to coextruded EPE encapsulants revealed their limitations. For EPE-1, residual enthalpy-based calculations showed a clear trend in crosslinking development, while G_{MF} values became unreliable due to the influence of the POE layer on the crystallization peak of EVA, producing apparent "over-curing" or false positive values. EPE-2 presented a different challenge; both layers are crosslinking polymers but with distinct curing rates. While G_e indicated high crosslinking and rapid peroxide decomposition, melt/freeze calculations were limited by a second crystallization peak in the second cooling curve.

These observations highlight that methods developed for monolayer encapsulants must be reconsidered and adapted for more complex, multilayer encapsulants. Furthermore, other quantitative techniques for assessing the degree of crosslinking in individual EVA or POE layers, such as gel content determination by Soxhlet extraction, will reach practical limits in applicability for multilayer EPE systems. Since both the soluble and insoluble fractions contain contributions from both polymers, the measured gel content reflects the combined behaviour of the laminate and does not allow direct determination of the crosslinking degree of the individual EVA and POE layers [68]. Accurate determination will therefore become considerably more challenging, requiring

detailed knowledge of layer composition, relative mass fractions, and individual crosslinking behaviour, particularly when components cure at different rates.

3.3 | PCA of FTIR-ATR Spectra of Encapsulants According to Lamination Duration

PCA of all crosslinking encapsulants revealed a systematic progression with increasing lamination duration, with samples generally shifting from right (0 min) to left (30 min) in the score plot (Figure 4). In the individual score plots, samples generally shifted along PC1 with increasing lamination duration. Samples laminated for 0–5 min were mostly located closer to the region associated with short lamination times, whereas samples laminated for 15–30 min were positioned towards the opposite end of PC1. Intermediate lamination durations generally occupied transitional positions, although the exact progression differed between encapsulants. For POE-1 and EPE-1, the 5 min samples remained relatively close to the samples exposed to shorter lamination durations, whereas for POE-2 and EPE-2, they had already shifted towards an intermediate position. For EVA, the 5 min samples occupied intermediate positions, while samples laminated for 10 min or longer were predominantly located in the high-lamination region, which is consistent with the trends observed by DSC. In contrast, POE-2 exhibited a stronger shift in the PCA score plot than suggested by the DSC-derived values.

PCA was used to assess trends and clustering in the FTIR data in relation to lamination duration and the associated material changes rather than to quantify crosslink density. The systematic progression of the samples with increasing lamination duration indicates that FTIR-PCA is sensitive to lamination-induced changes, such as decomposition of peroxides and decrease in crystallinity. As the complete spectra were included, the observed clustering reflects overall spectral changes rather than variations in a single band. The PCA results generally followed trends similar to those obtained from the DSC-based G_{MF} calculations, despite the limitations and inconsistencies observed for some encapsulants in the DSC analysis.

It is important to note that FTIR-ATR is a surface-sensitive technique with a penetration depth limited to only a few micrometres. Consequently, for the EPE encapsulants, the PCA results should be interpreted as reflecting changes occurring predominantly at the encapsulant surface (EVA layer). More generally, for all investigated materials, FTIR-PCA should be regarded as a qualitative and comparative tool for identifying lamination-related trends rather than as a quantitative measure of the overall degree of crosslinking.

3.4 | Thermomechanical Behaviour of Unlaminated (Uncured) Encapsulants

The CTE measurements of the unlaminated encapsulants revealed pronounced differences in dimensional stability, reflecting variations in the initial material state of the investigated encapsulants that are likely associated with differences in their manufacturing history.

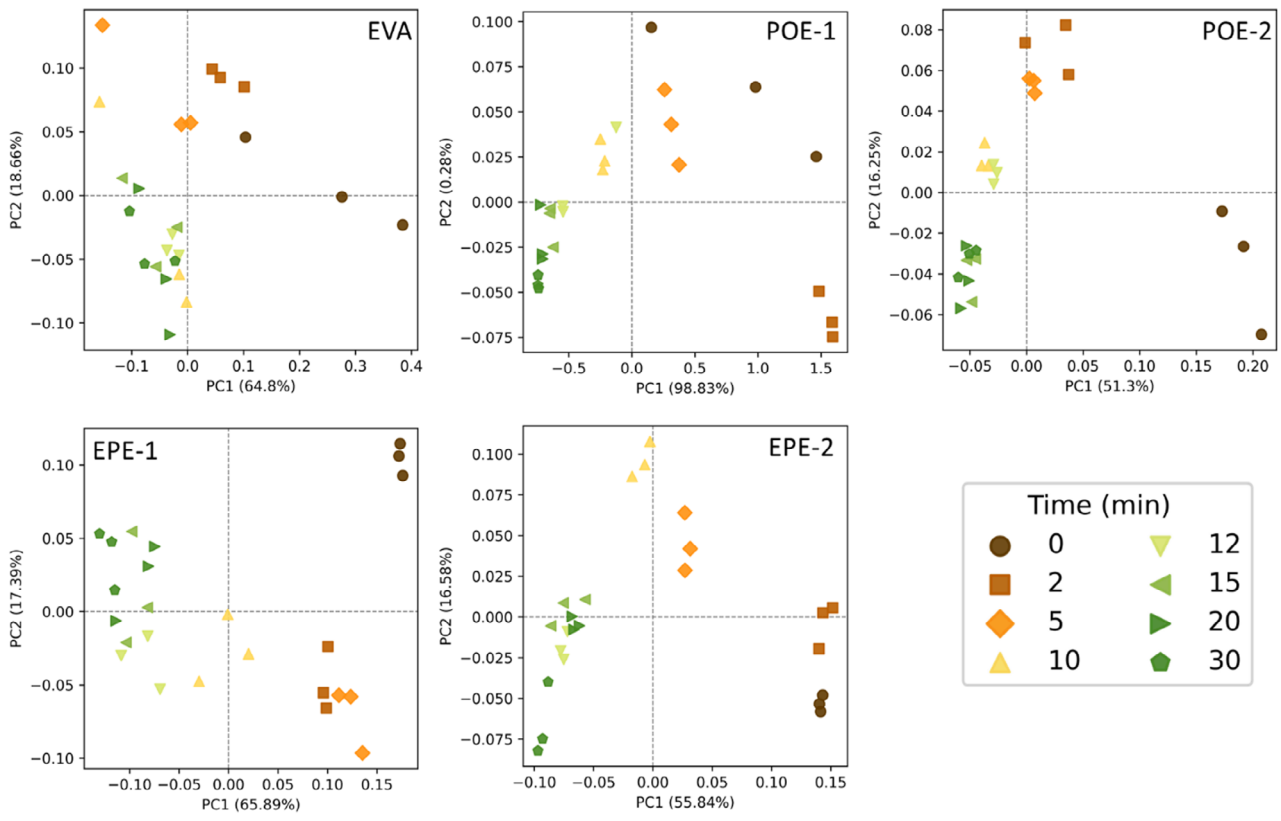

FIGURE 4 | PCA scatter plots of PC1 versus PC2 for all crosslinking encapsulants at different lamination times.

Figure 5 shows the in-plane dimensional changes calculated from horizontal and vertical gauge lines taken from the centre of the samples, each with an initial length of 20 mm. Figure 6 presents the CTE evaluated over the central area of the sample, represented by a regular grid (see the red mesh in Figure 7a), in the temperature range from 20 to 120 °C for all investigated unlaminated encapsulants, in both the MD and the TD. Dimensional stability (i.e., shrinkage and expansion) is directly related to the CTE as the latter is derived from the measured dimensional changes.

EVA encapsulant exhibited shrinkage in both directions over the measured temperature range. As the material contracted in-plane, a corresponding increase of 0.15 mm in thickness was observed, indicating material flow towards the interior. Shrinkage was more pronounced in the MD, while a reduction in shrinkage rate was observed at temperatures around 90 °C.

Although POE-1 and POE-2 belong to the same material class, significant differences in their dimensional response were observed. POE-1 showed strong shrinkage in the MD, accompanied by

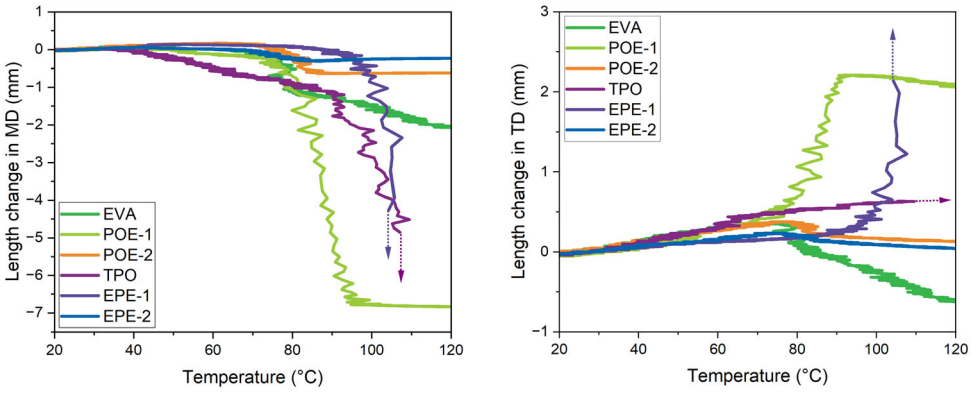

FIGURE 5 | Dimensional (length) change in machine (MD) (left) and transverse (TD) (right) direction for unlaminated encapsulants. Dotted arrows point the visually observed shrinkage or expansion trends for TPO and EPE-1, beyond the data measured by DIC.

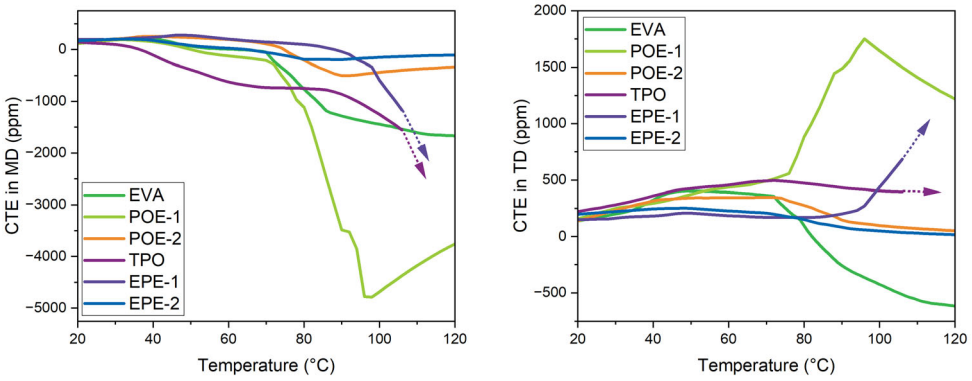

FIGURE 6 | CTE in machine (MD) (left) and transverse direction (TD) (right) for unlaminated encapsulants. Dotted arrows point the CTE behaviour trends for TPO and EPE-1, beyond the data measured by DIC.

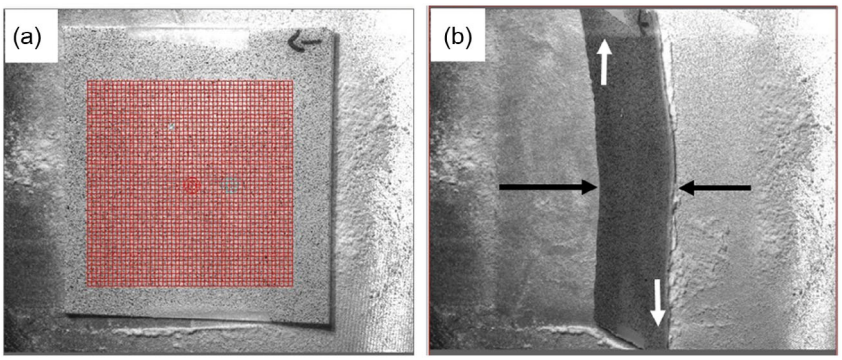

FIGURE 7 | Unlaminated EPE-1 before ((a) 4 cm width) and after ((b) ≈1.5 cm width) CTE measurements, shrinkage in machine (black arrows) and expansion in transverse direction (white arrows).

expansion in the TD. The magnitude of shrinkage considerably exceeded the transverse expansion and was accompanied by an increase in specimen thickness from ≈0.45 to 1.0 mm after the thermal cycle. This behaviour is consistent with relaxation of anisotropy introduced during film manufacturing (a schematic illustration of the proposed evolution of the encapsulant polymer structure during manufacturing and lamination process is provided in the Supporting Information (Figure S13)). In contrast, POE-2 exhibited substantially lower dimensional changes in both directions, with shrinkage magnitudes approximately eleven times lower than those observed for POE-1, suggesting that the material entered the lamination process in a more dimensionally stable initial state.

TPO, as the only single-layer thermoplastic encapsulant investigated, experienced pronounced shrinkage in the MD once the melting onset temperature was reached. Above ≈105 °C, the applied speckle pattern could no longer be tracked by DIC due to excessive deformation caused by encapsulant warping, and no further quantitative data could be obtained. Nevertheless, visual observation confirmed continued shrinkage in the MD. Only a minor expansion was observed in the TD.

EPE-1, containing a TPO core layer, exhibited the largest dimensional changes among all investigated encapsulants. A pronounced shrinkage was observed in MD, while expansion in TD was higher than that for the other materials. The in-plane contraction was accompanied by a substantial increase in thickness from ≈0.45 to 1.5 mm, indicating significant 3D redistribution of material during the heating. In Figure 7, the dimensional change of EPE-1 specimen can be seen after the heating and cooling step, and observable shrinkage corresponds to the combined shrinkage occurred during heating and additional shrinkage that took place during the cooling stage.

Among all investigated materials, EPE-2 demonstrated the highest dimensional stability. Only a minor shrinkage was observed in MD directions (−0.23 mm or 1.1%). The substantially lower dimensional changes compared to EPE-1 indicate that significant differences in thermomechanical behaviour can exist between encapsulants under the same name label, further emphasizing the influence of the initial material state on the subsequent thermomechanical response.

The pronounced dimensional changes observed in the unlaminated encapsulants demonstrate that the manufacturing-induced initial material state can strongly influence thermomechanical behaviour during the evacuation heating stage of lamination (see Figure S13 for the lamination stages). This stage is particularly challenging because shrinkage can occur before the encapsulant becomes constrained by the fully laminated module stack, which may contribute to manufacturing-related defects as illustrated in Figure 1, where excessive dimensional changes cause local deformation of the laminate.

The measured dimensional changes were substantially larger than shrinkage values typically reported in technical datasheets, highlighting the importance of evaluating encapsulant behaviour under conditions representative of PV module processing, for example, following IEC 62788-1-5 *Encapsulants—Measurement of change in linear dimensions of sheet encapsulation material resulting from applied thermal conditions* [84]. Furthermore, the observed differences were not limited to comparisons between material classes but were also found among encapsulants belonging to the same nominal material family. This demonstrates that generic material classification alone is insufficient to predict thermomechanical behaviour prior to lamination and emphasizes the importance of considering the manufacturing-induced initial material state when selecting encapsulants for PV module applications.

These findings are particularly relevant for emerging PV module architectures, including glass-free, lightweight, flexible, and silicon-perovskite tandem modules, where encapsulant dimensional changes are less constrained and where thermomechanical mismatches may have a greater influence on manufacturing yield and long-term reliability. Collectively, the results highlight the importance of evaluating encapsulant materials not only based on chemistry, adhesion, or barrier properties but also on their dimensional stability prior to lamination.

3.5 | Thermomechanical Behaviour of Laminated (Cured) Encapsulants

Following lamination, thermomechanical behaviour reflects the gradual transformation of the manufacturing-induced initial material state into a new laminated state through polymer chain relaxation, reorientation, and, for crosslinking encapsulants, network formation, as described and schematically presented in Supporting Information.

A lamination duration of 2 min substantially altered the dimensional response of all materials relative to the unlaminated state (see Figure 8). The anisotropic behaviour observed in the unlaminated encapsulants, characterized by shrinkage in MD and expansion in TD, was reduced after lamination. However, 2 min was insufficient to allow complete relaxation and reorientation of polymer chains in the molten state, and DSC results indicated that only limited crosslinking had occurred in the crosslinking encapsulants. Nevertheless, a pronounced change in dimensional behaviour was observed. Following heating and pressure application during lamination, the thermomechanical response shifted from the MD-shrinkage/TD-expansion behaviour of the unlaminated materials towards predominantly MD-shrinkage/TD-shrinkage, i.e., contraction occurring in both directions.

Among the investigated materials, EVA exhibited the largest dimensional changes after 2 min of lamination. In contrast, POE-1, which showed pronounced shrinkage in the unlaminated state, displayed a considerably more stable response after lamination. Similar reductions in dimensional change were observed for TPO, EPE-1, and POE-2. EPE-2 remained the most dimensionally stable encapsulant, exhibiting only minor shrinkage in both directions.

Increasing lamination duration further reduced the magnitude of dimensional changes and the differences between MD and TD CTE values (see Figures 9 and S7–S12). A lamination duration of 5 min was insufficient to achieve final thermomechanical response for EVA, POE-1, and POE-2, nearly sufficient for

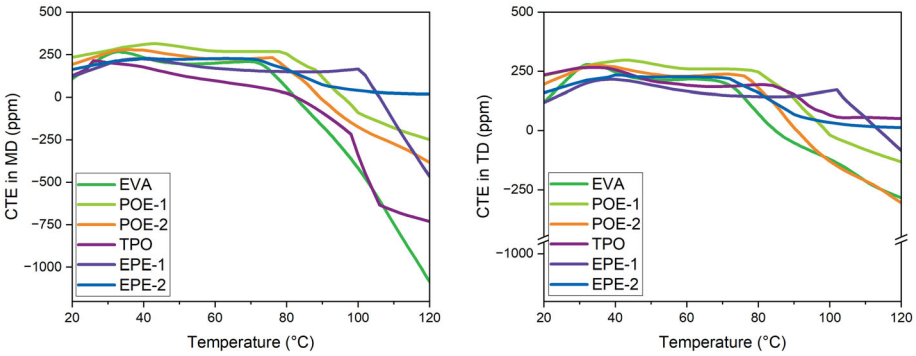

FIGURE 8 | CTE curves in machine (MD) (left) and transverse direction (TD) (right) of 2 min laminated encapsulants.

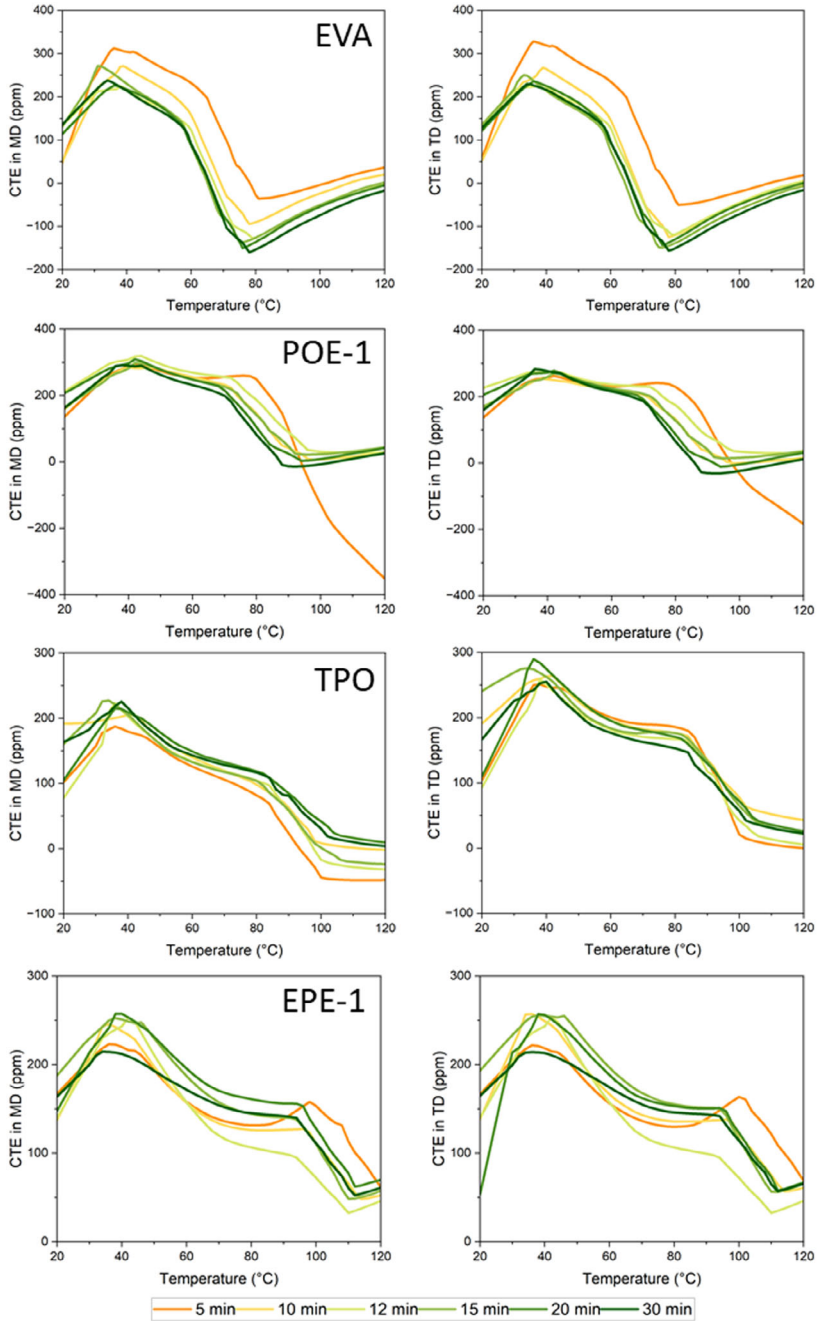

FIGURE 9 | CTE curves in in machine (MD) (left) and transverse (TD) (right) direction of 5–30 min laminated EVA, POE-1, TPO, and EPE-1 samples.

TPO and EPE-1, and close to sufficient for EPE-2. POE-1 exhibited highest shrinkage in both directions, suggesting a need for longer lamination times at 150 °C for polymer chain reorientation and higher crosslinking degree.

While encapsulants obtained "final" thermomechanical properties for ≥10 min of lamination duration, material-dependent differences in the time required to reach a stable thermomechanical response were evident. TPO, EPE-1, and EPE-2 approached stable behaviour at shorter lamination durations, whereas EVA, POE-1, and POE-2 continued to exhibit measurable changes up to ≈12 min. These observations indicate that the evolution of thermomechanical behaviour during lamination depends not only on the polymer type but also on the initial state of the encapsulant entering the lamination process and, for crosslinking materials, on the progression of network formation observed by DSC.

A small difference in the shape of the CTE curve was observed for EPE-1 laminated for 12 min. DSC analysis of this specimen indicated a lower fraction of the POE core layer compared with the other EPE-1 samples, suggesting that variations in layer distribution may influence the thermomechanical response of coextruded encapsulants. While the effect was relatively small, it demonstrates the additional complexity associated with multilayer encapsulants.

The thermomechanical behaviour of all six encapsulants laminated for 30 min is compared in Figure 10. Clear differences in CTE values and temperature-dependent dimensional changes are observed between all studied materials, not only between different polymer types but also within the same material groups, as shown by the variation between POE-1 and POE-2 and between EPE-1 and EPE-2. Despite these differences between materials, overlapping the CTE curves measured in MD and TD shows that all encapsulants individually display nearly isotropic behaviour after 30 min of lamination. Compared to the initial state and shorter lamination times, this indicates that longer lamination improves the uniformity of the thermomechanical response.

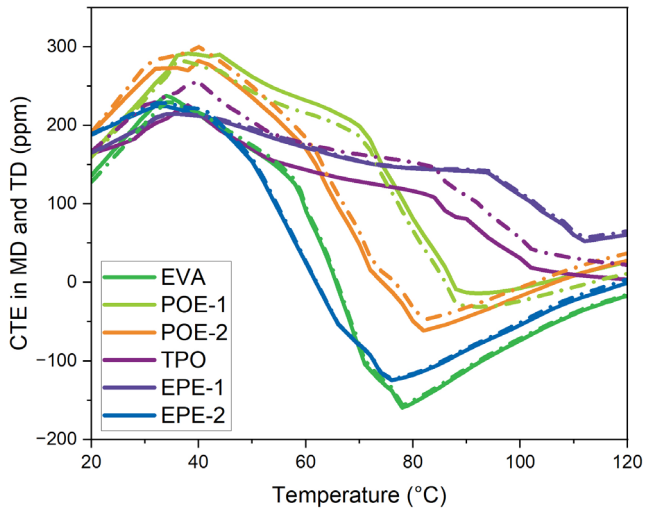

FIGURE 10 | CTE curves in machine (solid line) and transverse direction (dash/dot line) of 30 min laminated encapsulants.

Interestingly, the encapsulants exhibiting the largest dimensional changes in the unlaminated state, TPO and EPE-1, displayed the lowest CTE range and only minor contraction above the melting temperature. This observation demonstrates that large dimensional relaxation during the initial heating stage does not necessarily translate into a less stable thermomechanical response after sufficient lamination. Instead, the results highlight the importance of evaluating both the initial state of the encapsulant and its evolution during lamination when assessing thermomechanical behaviour.

Crosslinking materials, EVA, POE-1, POE-2, and EPE-2, exhibit CTE values ranging from ≈300 to −150 ppm across the measured temperature range, together with noticeable contraction in the melting region, which can be linked to remaining noncrosslinked polymer fractions. These results highlight the strongly temperature-dependent nature of encapsulant thermomechanical behaviour. Consequently, the measured behaviour may be relevant for future efforts aimed at improving the realism of thermomechanical modelling of PV modules.

Although the measurements were performed on unconstrained encapsulants, the observed thermomechanical behaviour provides insight into dimensional changes and stress development that may occur during PV module manufacturing and operation. Dimensional changes occurring during the early stages of lamination contribute to the initial stress state of the laminate, while subsequent thermal cycling during field exposure may further amplify stresses arising from thermomechanical mismatches between module components.

4 | Conclusions

This study investigated the influence of the manufacturing-induced initial material state and lamination duration on the thermomechanical behaviour of six commercially relevant PV encapsulants, including EVA, POE, TPO, and coextruded EPE materials.

Significant differences in thermomechanical behaviour were observed not only between encapsulant classes but also between materials belonging to the same nominal material family. These results demonstrate that generic material classification alone is insufficient to predict dimensional stability and thermomechanical response during PV module manufacturing.

Both DSC (combined residual enthalpy and melt/freeze methods) and FTIR-ATR/PCA revealed limitations regarding the characterization of crosslinking behaviour of coextruded multilayer EPE encapsulants. DSC-based approaches provided useful information on curing progression but were influenced by residual peroxide content, crystallization behaviour, and multilayer material architecture (EVA and POE distribution in the stack). FTIR-ATR combined with PCA proved to be a useful nondestructive tool for qualitative assessment of material evolution during lamination; however, FTIR-ATR measures only the surface, limiting assessment only to the outer EVA layers.

DIC measurements revealed substantial differences in dimensional stability between unlaminated encapsulants, reflecting

differences in their manufacturing-induced initial material state. During unconstrained heating, these differences manifested as pronounced shrinkage and anisotropic dimensional changes, indicating that the initial state of the encapsulant can strongly influence behaviour during the early stages of lamination.

Lamination progressively modified this initial state and reduced thermomechanical anisotropy. Depending on the material, ≈5–10 min of lamination at 150 °C was required to achieve stable thermomechanical behaviour. Interestingly, the encapsulants exhibiting the largest dimensional changes prior to lamination, namely, TPO and EPE-1, displayed the lowest CTE range after extended lamination, highlighting the importance of evaluating both the initial state and the evolution of encapsulant properties during processing.

Although the measurements were performed on unconstrained encapsulants, the results provide experimental insight into dimensional changes occurring during lamination and into the temperature-dependent thermomechanical behaviour of postlaminated encapsulants. The presented dataset may support future investigations of stress development, thermomechanical interactions, and material selection in conventional and emerging PV module architectures.

Acknowledgments

This work was conducted as part of the Austrian "e!MISSION.at—Energy Mission Austria" project "PV Industriefassade" (FFG No. FO999915062) funded by the Austrian Climate and Energy Fund and the Austrian Research Promotion Agency (FFG).

This research project (grant number: 911658) was funded by COMET—Competence Centers for Excellent Technologies—through BMIMI, BMWET, and the cofinancing federal provinces (Styria through SFG, Upper Austria, Vorarlberg) and carried out with the participation of scientific and company partners. The COMET program is managed by FFG.

The authors would like to acknowledge Ivaylo Mitev for his advice for sample preparation and CTE measurements and Christian Veas and Lisa Maitz for their assistance with nondestructive spectroscopic measurements.

Open Access funding provided by Montanuniversitat Leoben.

Funding

This study was supported by Austrian Climate and Energy Fund and the Austrian Research Promotion Agency (Grant FO999915062), COMET—Competence Centers for Excellent Technologies (Grant 911658).

Conflicts of Interest

The authors declare no conflicts of interest.

Data Availability Statement

The data that support the findings of this study are available on request from the corresponding author.

References

1. VDMA e.V. Photovoltaics Equipment, ed. *International Technology Roadmap for Photovoltaics (ITRPV)*, 16th ed. (2025).

2. G. Oreski, C. Barretta, P. Christöfl, et al., "What Is a Polyolefin? A Critical Overview of Ethylene Copolymers Used as Solar Photovoltaic Module Encapsulants," *Progress in Photovoltaics: Research and Applications* 34 (2026): 367–395, https://doi.org/10.1002/pip.70038.

3. J. Zuboy, M. Springer, E. C. Palmiotti, et al., "Getting Ahead of the Curve: Assessment of New Photovoltaic Module Reliability Risks Associated With Projected Technological Changes," *IEEE Journal of Photovoltacis* 14 (2024): 4–22.

4. Intersolar, "Solar Technology Is Undergoing Great Changes: Market Trend—January 28, 2025," (2025), accessed December 10, 2025, https://www.intersolar.de/market-trends/solar-cell-development.

5. T. J. Silverman, E. C. Palmiotti, M. Springer, et al., *Tough Break: Many Factors Make Glass Breakage More Likely* (2024).

6. G. Oreski, J. S. Stein, G. C. Eder, et al., "Motivation, Benefits, and Challenges for New Photovoltaic Material & Module Developments," *Progress in Energy* 4 (2022): 32003, https://doi.org/10.1088/2516-1083/ac6f3f.

7. S. K. Chunduri and M. Schmela, *TaiyangNews Solar Backsheets & Encapsulants Market Survey 2024/25* (2025).

8. N. Pervan, G. Eder, Y. Voronko, et al., "Is EPE the Future of PV Encapsulation? A Comprehensive Material-Level Assessment," *Solar Energy Materials and Solar Cells* 300 (2026): 114258, https://doi.org/10.1016/j.solmat.2026.114258.

9. G. Kakoulaki, R. Kenny, N. Taylor, et al., "Mapping Europe's Rooftop Photovoltaic Potential With a Building-Level Database," *Nature Energy* 11 (2026): 324–333, https://doi.org/10.1038/s41560-025-01947-x.

10. M. Deshaies, "Problèmes géographiques des transitions énergétiques quelles perspectives pour l'évolution du système énergétique?," *Transition énergétique et développement* (2020): 25–44.

11. J. M. Kiesecker, J. S. Evans, J. R. Oakleaf, et al., "Land use and Europe's Renewable Energy Transition: Identifying Low-Conflict Areas for Wind and Solar Development," *Frontiers in Environmental Science* 12 (2024): 1355508, https://doi.org/10.3389/fenvs.2024.1355508.

12. M. Trommsdorff, P. E. Campana, J. Macknick, A. Fernández Solas, S. Gorjian, and I. Tsanakas, *Dual Land Use for Agriculture and Solar Power Production: Overview and Performance of Agrivoltaic Systems* (International Energy Agency Photovoltaic Power Systems Programme, 2025).

13. J. Selj, S. Wieland, and I. Tsanakas, *Floating Photovoltaic Power Plants: A Review of Energy Yield, Reliability, and Maintenance* (International Energy Agency Photovoltaic Power Systems Programme, 2025).

14. IEA PVPS, *Successful Building Integration of Photovoltaics—A Collection of International Projects* (International Energy Agency, 2021).

15. K. Araki, A. J. Carr, F. Chabuel, et al., *State-of-the-Art and Expected Benefits of PV-Powered Vehicles: Report IEA-PVPS T17-01 2021* (2021).

16. P. Gebhardt, U. Kräling, E. Fokuhl, I. Hädrich, and D. Philipp, "Reliability of Commercial TOPCon PV Modules—An Extensive Comparative Study," *Progress in Photovoltaics: Research and Applications* 33 (2024): 1378, https://doi.org/10.1002/pip.3868.

17. C. Sen, H. Wang, M. U. Khan, et al., "Buyer Aware: Three New Failure Modes in TOPCon Modules Absent From PERC Technology," *Solar Energy Materials and Solar Cells* 272 (2024): 112877, https://doi.org/10.1016/j.solmat.2024.112877.

18. M. Babin, G. C. Eder, Y. Voronko, and G. Oreski, "Water Vapor Permeability of Polymeric Packaging Materials for Novel Glass-Free Photovoltaic Applications," *Journal of Applied Polymer Science* 141 (2024): e55733, https://doi.org/10.1002/app.55733.

19. P. Subudhi and D. Punetha, "Pivotal Avenue for Hybrid Electron Transport Layer-Based Perovskite Solar Cells With Improved Efficiency," *Scientific Reports* 13 (2023): 19485, https://doi.org/10.1038/s41598-023-33419-1.

20. S. Zhang, Z. Liu, W. Zhang, et al., "Barrier Designs in Perovskite Solar Cells for Long-Term Stability," *Advanced Energy Materials* 10 (2020): 2001610, https://doi.org/10.1002/aenm.202001610.

21. H. Jiao, M. Hegde, N. Li, et al., "Metal Halide Perovskite Solar Module Encapsulation Using Polyolefin Elastomers: The Role of Morphology in Preventing Delamination," *PRX Energy* 3 (2024): 023013, https://doi.org/10.1103/PRXEnergy.3.023013.

22. M. de Bastiani, G. Armaroli, R. Jalmood, et al., "Mechanical Reliability of Fullerene/Tin Oxide Interfaces in Monolithic Perovskite/Silicon Tandem Cells," *ACS Energy Letters* 7 (2022): 827–833, https://doi.org/10.1021/acsenergylett.1c02148.

23. C. Peike, I. Häldrich, K.-A. Weiß, and I. Dürr, "Overview of PV Module Encapsulation Materials," *Photovoltaics International* 19 (2013): 85–92.

24. A. W. Czanderna and F. J. Pern, "Encapsulation of PV Modules Using Ethylene Vinyl Acetate Copolymer as a Pottant: A Critical Review," *Solar Energy Materials and Solar Cells* 43 (1996): 101–181, https://doi.org/10.1016/0927-0248(95)00150-6.

25. E. Özkalay, G. Friesen, M. Caccivio, et al., "Operating Temperatures and Diurnal Temperature Operating Temperatures and Diurnal Temperature Variations of Modules Installed in Open-Rack and Typical BIPV Configurations," *IEEE Journal of Photovoltacis* 12 (2022): 133–140.

26. M. Köntges, G. Oreski, U. Jahn, et al., *Assessment of Photovoltaic Module Failures in the Field: Report IEA-PVPS T13-09:2017* (2017).

27. U. Erdil, M. Khenkin, W. M. Bernardes de Araujo, et al., "Delamination of Perovskite Solar Cells in Thermal Cycling and Outdoor Tests," *Energy Technology* 13 (2025): 2401280, https://doi.org/10.1002/ente.202401280.

28. H. Bristow, X. Li, M. Babics, et al., "Mitigating Delamination in Perovskite/Silicon Tandem Solar Modules," *Solar RRL* 8 (2024): 2400289, https://doi.org/10.1002/solr.202400289.

29. M. Herz, G. Friesen, U. Jahn, M. Köntges, S. Lindig, and D. Moser, "*Quantification of Quantification of Technical Risks in PV Power Systems: IEA PVPS Task 13, Report IEA-PVPS T13-23:2021* (2021).

30. S. Y. Lee, *Thermomechanical Properties of Polymeric Materials and Related Stresses* (1990).

31. V. Bourg, P. Ienny, A. S. Caro-Bretelle, N. Le Moigne, V. Guillard, and A. Bergeret, "Modeling of Internal Residual Stress in Linear and Branched Polyethylene Films During Cast Film Extrusion: Towards a Prediction of Heat-Shrinkability," *Journal of Materials Processing Technology* 271 (2019): 599–608, https://doi.org/10.1016/j.jmatprotec.2019.04.002.

32. T.-I. Lee, M. S. Kim, and T.-S. Kim, "Contact-Free Thermal Expansion Measurement of Very Soft Elastomers Using Digital Image Correlation," *Polymer Testing* 51 (2016): 181–189, https://doi.org/10.1016/j.polymertesting.2016.03.014.

33. T. W. Womer, "Optimizing Sheet Extrusion Conditions to Minimize Internal Stresses in Thermoformed Sheet," *Journal of Plastic Film & Sheeting* 8 (1992): 26–36, https://doi.org/10.1177/875608799200800104.

34. N. Saba and M. Jawaid, "A Review on Thermomechanical Properties of Polymers and Fibers Reinforced Polymer Composites," *Journal of Industrial and Engineering Chemistry* 67 (2018): 1–11, https://doi.org/10.1016/j.jiec.2018.06.018.

35. L. Eyann, M. A. Fatah Muhamed Mukhtar, A. A. Saad, and M. Jaafar, "Epoxy Molding Compounds for High-Performance Electronic Packaging: A Review on Recent Studies," *Materials Science in Semiconductor Processing* 197 (2025): 109665, https://doi.org/10.1016/j.mssp.2025.109665.

36. T. Tetsuya, Y. Hashimoto, U. S. Ishiaku, M. Mizoguchi, Y. W. Leong, and H. Hamada, "Effect of Heat-Sealing Temperature on the Properties of OPP/CPP Heat Seals. Part II. Crystallinity and Thermomechanical Properties," *Journal of Applied Polymer Science* 99 (2006): 513–519, https://doi.org/10.1002/app.22443.

37. S. Pisani, I. Genta, T. Modena, R. Dorati, M. Benazzo, and B. Conti, "Shape-Memory Polymers Hallmarks and Their Biomedical Applications in the Form of Nanofibers," *International Journal of Molecular Sciences* 23 (2022): 1290, https://doi.org/10.3390/ijms23031290.

38. J.-H. Park, E. Lee, I.-D. Kim, et al., "A Review of the Thermo-Mechanical Analysis Framework for Microelectronics Packaging: Mechanics, Material Property Determination, and Structural Considerations," *Materials Science in Semiconductor Processing* 205 (2026): 110321, https://doi.org/10.1016/j.mssp.2025.110321.

39. A. G. Khina, D. P. Bulkatov, I. P. Storozhuk, and A. P. Sokolov, "Coefficient of Linear Thermal Expansion of Polymers and Polymer Composites: A Comprehensive Review," *Polymers* 17 (2025): 3097, https://doi.org/10.3390/polym17233097.

40. M. Knausz, G. Oreski, M. Schmidt, et al., "Thermal Expansion Behavior of Solar Cell Encapsulation Materials," *Polymer Testing* 44 (2015): 160–167, https://doi.org/10.1016/j.polymertesting.2015.04.009.

41. G. Oreski, A. Rauschenbach, C. Hirschl, M. Kraft, G. C. Eder, and G. Pinter, "Crosslinking and Post-Crosslinking of Ethylene Vinyl Acetate in Photovoltaic Modules," *Journal of Applied Polymer Science* 134 (2017): 101, https://doi.org/10.1002/app.44912.

42. P. Romer, G. Oreski, A. J. Beinert, H. Neuhaus, and M. Mittag, "More Realistic Considerations of Backsheets Coefficient of Themal Expansion on Thermomechanics of PV Modules," in 37th European Photovoltaic Solar Energy Conference and Exhibition (2020), 772–776.

43. N. Bosco, M. Springer, and X. He, "Viscoelastic Material Characterization and Modeling of Photovoltaic Module Packaging Materials for Direct Finite-Element Method Input," *IEEE Journal of Photovoltaics* 10 (2020): 1424–1440, https://doi.org/10.1109/JPHOTOV.2020.3005086.

44. V. Meslier, B. Chambion, P.-O. Bouchard, and J.-L. Bouvard, "Thermal Expansion Behavior of a Thermoplastic Polyolefin for Photovoltaic Application Over Hygrothermal Aging," *IEEE Journal of Photovoltaics* 14 (2024): 1–10, https://doi.org/10.1109/JPHOTOV.2024.3463950.

45. V. Meslier, J.-L. Bouvard, P.-O. Bouchard, B. Chambion, and A. Derrier, "Measurement of Encapsulant Thermal Expansion (CTE): Impact of Residual Stresses," in 41st European Photovoltaic Solar Energy Conference and Exhibition, 3AV.1.13.

46. P. Nivelle, J. A. Tsanakas, J. Poortmans, and M. Daenen, "Stress and Strain Within Photovoltaic Modules Using the Finite Element Method: A Critical Review," *Renewable and Sustainable Energy Reviews* 145 (2021): 111022, https://doi.org/10.1016/j.rser.2021.111022.

47. A. J. Beinert, P. Romer, A. Büchler, V. Haueisen, J. Aktaa, and U. Eitner, "Thermomechanical Stress Analysis of PV Module Production Processes by Raman Spectroscopy and FEM Simulation," *Energy Procedia* 124 (2017): 464–469, https://doi.org/10.1016/j.egypro.2017.09.282.

48. S. K. Tippabhotla, W. Song, A. A. Tay, and A. S. Budiman, "Effect of Encapsulants on the Thermomechanical Residual Stress in the Back-Contact Silicon Solar Cells of Photovoltaic Modules—A Constrained Local Curvature Model," *Solar Energy* 182 (2019): 134–147, https://doi.org/10.1016/j.solener.2019.02.028.

49. U. Eitner, S. Kajari-Schröder, M. Köntges, and H. Altenbach, Thermal Stress and Strain of Solar Cells in Photovoltaic Modules, in *Shell-Like Structures*, ed. H. Altenbach and V. A. Eremeyev (Springer, 2011): 453–468.

50. M. Paggi, S. Kajari-Schröder, and U. Eitner, "Thermomechanical Deformations in Photovoltaic Laminates," *Journal of Strain Analysis for Engineering Design* 46 (2011): 772–782, https://doi.org/10.1177/0309324711421722.

51. N. Klasen, F. Heinz, A. de Rose, T. Roessler, A. Kraft, and M. Kamlah, "Root cause Analysis of Solar Cell Cracks at Shingle Joints," *Solar Energy Materials and Solar Cells* 238 (2022): 111590, https://doi.org/10.1016/j.solmat.2022.111590.

52. A. J. Beinert, P. Romer, M. Heinrich, M. Mittag, J. Aktaa, and D. H. Neuhaus, "The Effect of Cell and Module Dimensions on

Thermomechanical Stress in PV Modules," *IEEE Journal of Photovoltaics* 10 (2020): 70–77, https://doi.org/10.1109/JPHOTOV.2019.2949875.

53. L. Papargyri, P. Papanastasiou, and G. E. Georghiou, "Sequential Thermomechanical Stress and Cracking Analysis of Photovoltaic Modules With Full and Half-Cut Cells," *Solar Energy Materials and Solar Cells* 278 (2024): 113166, https://doi.org/10.1016/j.solmat.2024.113166.

54. M. Pander, S. Dietrich, S.-H. Schulze, U. Eitner, and M. Ebert, "Thermo-Mechanical Assessment of Solar Cell Displacement With Respect to the Viscoelastic Behaviour of the Encapsulant," in 12th International Thermal, Mechanical and Multi-Physics Simulation and Experiments in Microelectronics and Microsystems, 433–438.

55. D. C. Miller, X. Gu, L. Ji, et al., "Examination of a Size-Change Test for Photovoltaic Encapsulation Materials," in *Reliability of Photovoltaic Cells, Modules, Components, and Systems V* (SPIE, 2012): 84720T.

56. Breyer GmbH, Green EVA Extrusion Line for Encapsulation Film: Advanced Technology Combines Low Shrinkage Encapsulation Film and High Production Speed—No Energy Consuming Annealing Necessary, No Interlayer Necessary (2026), accessed February 18, 2026.

57. G. Oreski, M. Knausz, G. Pinter, C. Hirschl, and G. C. Eder, "Advanced Methods for Discovering PV Module Process Optimization Potentials and Quality Control of Encapsulation Materials," in 28th European Photovoltaic Solar Energy Conference and Exhibition (2013).

58. H.-Y. Li, L.-E. Perret-Aebi, V. Chapuis, C. Ballif, and Y. Luo, "The Effect of Cooling Press on the Encapsulation Properties of Crystalline Photovoltaic Modules: Residual Stress and Adhesion," *Progress in Photovoltaics* 23 (2015): 160–169, https://doi.org/10.1002/pip.2409.

59. C. Hirschl, M. Biebl–Rydlo, M. DeBiasio, et al., "Determining the Degree of Crosslinking of Ethylene Vinyl Acetate Photovoltaic Module Encapsulants—A Comparative Study," *Solar Energy Materials and Solar Cells* 116 (2013): 203–218, https://doi.org/10.1016/j.solmat.2013.04.022.

60. G. Oreski, M. Bredacs, S. Feldbacher, et al., "New Rapid Method for Optical Non-Destructive Determination of the Degree of Crosslinking of PV Module Encapsulants," in *2025 IEEE 53rd Photovoltaic Specialists Conference (PVSC)* (IEEE, 2025), 90–93.

61. J. C. Schlothauer, C. Peter, C. Hirschl, G. Oreski, and B. Röder, "Non-Destructive Monitoring of Ethylene Vinyl Acetate Crosslinking in PV-Modules by Luminescence Spectroscopy," *Journal of Polymer Research* 24 (2017): 203, https://doi.org/10.1007/s10965-017-1409-y.

62. G. M. Wallner, B. Adothu, R. Pugstaller, F. R. Costa, and S. Mallick, "Comparison of Crosslinking Kinetics of UV-Transparent Ethylene-Vinyl Acetate Copolymer and Polyolefin Elastomer Encapsulants," *Polymers* 14 (2022): 1441, https://doi.org/10.3390/polym14071441.

63. R. Meier, I. M. Slauch, and M. I. Bertoni, "Ultrasonic Characterization of Ethylene Vinyl Acetate (EVA) Crosslinking for Quality Assurance and Lamination Process Control," in 2023 IEEE 50th Photovoltaic Specialists Conference (PVSC) (IEEE, 2023), 1–5.

64. K. Agroui, G. Collins, G. Oreski, M. Boehning, A. Hadj Arab, and D. Ouadjaout, "Effect of Crosslinking on EVA-Based Encapsulant Properties During Photovoltaic Module Fabrication Process," *Journal of Renewable Energies* 18 (2023): 303, https://doi.org/10.54966/jreen.v18i2.508.

65. M. Jaunich, M. Böhning, U. Braun, G. Teteris, and W. Stark, "Investigation of the Curing State of Ethylene/Vinyl Acetate Copolymer (EVA) for Photovoltaic Applications by Gel Content Determination, Rheology, DSC and FTIR," *Polymer Testing* 52 (2016): 133–140, https://doi.org/10.1016/j.polymertesting.2016.03.013.

66. C. Hirschl, L. Neumaier, W. Mühleisen, et al., "In-Line Determination of the Degree of Crosslinking of Ethylene Vinyl Acetate in PV Modules by Raman Spectroscopy," *Solar Energy Materials and Solar Cells* 152 (2016): 10–20, https://doi.org/10.1016/j.solmat.2016.03.019.

67. S. Lust, T. Weber, S. R. Kuntamukkula, A. Mordvinkin, and M. Wendt, "Update of Quality Control Tests for New PV Encapsulation Materials," *EPJ Photovoltaics* 15 (2024): 5, https://doi.org/10.1051/epjpv/2024006.

68. A. Trefzer, A. K. Öz, J. Forster, C. Wellens, M. Çalışkan Arslan, and C. Düz, "Optimization of Soxhlet Extraction Parameters for Gel Content Determination of Co-Extruded EPE. WIP-Munich," in 42nd European Photovoltaic Solar Energy Conference and Exhibition (2025), https://doi.org/10.4229/EUPVSEC2025/3AV.1.18.

69. K. Liu, D. C. Miller, N. Bosco, and R. H. Dauskardt, "Determining the Crosslinking and Degradation Reaction Kinetics in Photovoltaic Encapsulants Using Accelerated Aging," in 2024 IEEE 52nd Photovoltaic Specialist Conference (PVSC) (IEEE, 2024), 909–914.

70. M. Landa-Pliquet, T. Béjat, M. Serasset, A. Descormes, E. Mofakhami, and E. Voroshazi, "Enhancing Photovoltaic Modules Encapsulation: Optimizing Lamination Processes for Polyolefin Elastomers (POE) Through Crosslinking Behavior Analysis," *Solar Energy Materials and Solar Cells* 267 (2024): 112725, https://doi.org/10.1016/j.solmat.2024.112725.

71. A. K. Öz, C. Herzog, C. Wellens, D. E. Mansour, M. Heinrich, and A. Kraft, "The Impact of the Lamination Process on the Adhesion Properties at the Glass-Encapsulant Interface and Damp Heat Stability of PV Modules," in 38th European Photovoltaic Solar Energy Conference and Exhibition, 708–714.

72. D. Wu, P. Wessel, J. Zhu, et al., "Influence of Lamination Conditions of EVA Encapsulation on Photovoltaic Module Durability," *Materials* 16 (2023): 6945, https://doi.org/10.3390/ma16216945.

73. S. Jonai, K. Hara, Y. Tsutsui, H. Nakahama, and A. Masuda, "Relationship Between Cross-Linking Conditions of Ethylene Vinyl Acetate and Potential Induced Degradation for Crystalline Silicon Photovoltaic Modules," *Japanese Journal of Applied Physics* 54 (2015): 08KG01, https://doi.org/10.7567/JJAP.54.08KG01.

74. J. Zhu, D. Montiel-Chicharro, T. R. Betts, and R. Gottschalg, Correlation of Degree of EVA Crosslinking With Formation and Discharge of Acetic Acid in PV Modules," in 33rd European Photovoltaic Solar Energy Conference and Exhibition, 1795–1798.

75. K. Liu, D. C. Miller, N. Bosco, J. M. Newkirk, and R. H. Dauskardt, ed., *Advancing Steady-State and Sequenced Accelerated Aging for Assessing the Adhesion Degradation of Contemporary Encapsulants* (2025).

76. G. Oreski, A. Rauschenbach, C. Hirschl, L. Neumaier, M. Kraft, and G. Pinter, "Challenges in Measuring the Degree of Crosslinking of Ethylene Vinyl Acetate," in 29th European Photovoltaic Solar Energy Conference and Exhibition (2014), 2457–2461, https://doi.org/10.4229/EUPVSEC20142014-5DO.10.2.

77. IEC, Measurement Procedures for Materials Used in Photovoltaic Modules—Part 1-6: Encapsulants—Test Methods for Determining the Degree of Cure in Ethylene-Vinyl Acetate, 1st ed. 27.160—Solar Energy Engineering (2017), accessed January 21, 2020, https://webstore.iec.ch/publication/33050.

78. G. James, D. Witten, T. Hastie, R. Tibshirani, and J. Taylor, *An Introduction to Statistical Learning: With Applications in R* (Springer, 2021).

79. J. F. Hair Jr, W. C. Black, B. J. Babin, and R. E. Anderson, *Multivariate Data Analysis*, 7th ed. (Pearson, 2009).

80. S. Ogier, C. Vidal, D. Chapron, et al., "A Comparative Study of Calorimetric Methods to Determine the Crosslinking Degree of the Ethylene-Co-Vinyl Acetate Polymer Used as a Photovoltaic Encapsulant," *Journal of Polymer Science Part B: Polymer Physics* 55 (2017): 866–876, https://doi.org/10.1002/polb.24335.

81. M. Hidalgo, F. Medlege, M. Vite, C. Corfias-Zuccalli, P. Voarino, and J. González-León, "A New DSC Method for the Quality Control of PV Modules: Simple and Quick Determination of the Degree of Crosslinking of EVA Encapsulants," *Photovoltaics International* 14 (2011): 131–137.

82. K. Brecl, C. Barretta, G. Oreski, B. Malic, and M. Topic, "The Influence of the EVA Film Aging on the Degradation Behavior of PV Modules Under High Voltage Bias in Wet Conditions Followed by Electroluminescence," *IEEE Journal of Photovoltaics* 9 (2019): 259–265, https://doi.org/10.1109/JPHOTOV.2018.2875196.

83. M. Wendt, P. Wessel, R. Gottschalg, A. Mordvinkin, and R. Heidrich, "Crosslinking Behavior of Ethylene-Vinyl Acetate Copolymer Encapsulants in Dependence of the Additive Composition," *Progress in Photovoltaics: Research and Applications* 33 (2024): 1322, https://doi.org/10.1002/pip.3849.

84. IEC, Measurement Procedures for Materials Used in Photovoltaic Modules—Part 1-5: Encapsulants—Measurement of Change in Linear Dimensions of Sheet Encapsulation Material Resulting From Applied Thermal Conditions 27.160—Solar Energy Engineering (2016), https://webstore.iec.ch/publication/25264.

Supporting Information

Additional supporting information can be found online in the Supporting Information section.